Journal of Power Sources 185 (2008) 1073–1078

Contents lists available at ScienceDirect

Journal of Power Sources

journal homepage: www.elsevier.com/locate/jpowsour

Performance of laboratory polymer electrolyte membrane hydrogen generator with sputtered iridium oxide anode

D. Labou [a,*], E. Slavcheva [b], U. Schnakenberg [c], S. Neophytides [a]

[a] Institute of Chemical Engineering and High Temperature Chemical Processes, Stadiou str., Platani 26504 Patras, Greece
[b] Institute of Electrochemistry and Energy Systems, Bulgarian Academy of Sciences, Sofia 1113, Bulgaria
[c] Institute of Materials in Electrical Engineering I, RWTH, Aachen University, D 52074 Aachen, Germany

ARTICLE INFO

Article history:
Received 30 April 2008
Received in revised form 8 July 2008
Accepted 3 August 2008
Available online 15 August 2008

Keywords:
PEM water electrolysis
Magnetron sputtering
Iridium oxides
Hydrogen production
Oxygen evolution reaction

ABSTRACT

The continuous improvement of the anode materials constitutes a major challenge for the future commercial use of polymer electrolyte membranes (PEM) electrolyzers for hydrogen production. In accordance to this direction, iridium/titanium films deposited directly on carbon substrates via magnetron sputtering are operated as electrodes for the oxygen evolution reaction interfaced with Nafion 115 electrolyte in a laboratory single cell PEM hydrogen generator. The anode with 0.2 mg cm^{-2} Ir catalyst loading was electrochemically activated by cycling its potential value between 0 and 1.2 V (vs. RHE). The water electrolysis cell was operated at 90 °C with current density 1 A cm^{-2} at 1.51 V without the ohmic contribution. The corresponding current density per mgr of Ir catalyst is 5 A mg^{-1}. The achieved high efficiency is combined with sufficient electrode stability since the oxidation of the carbon substrate during the anodic polarization is almost negligible.

1. Introduction

The benefits of the electrolyzed hydrogen which make it competitive to the hydrogen produced from hydrocarbons include primarily the excellent product purity as well as the possibility to produce it *on site* and *on demand* avoiding the transportation and storage problems. The majority of commercial electrolyzer systems belongs to the alkaline where an aqueous potassium hydroxide electrolyte circulates continuously through the electrolytic cells. In recent years, there is a growing interest in the acidic type electrolysis via proton conducting polymer membranes (PEM). PEM electrolyzers offer higher current densities (up to 10 kA m^{-2}) compared to the alkaline systems (2–5 kA m^{-2}) [1,2] since the requirement of a non-liquid electrolyte simplifies the design and balance of the plant. The main drawback of proton conducting PEM electrolysis is the relatively higher anodic overpotential during the oxygen evolution reaction (OER) with respect to alkaline process. During the last 15 years the higher performances reported in the field of PEM electrolyzers (T_{max} = 90 °C) were established on Ir, Pt–Ir, Ir–Ru and Ir–Ta oxides, while Ir–Ru has been proven to be the most active O_2 evolution electrocatalyst [3–12]. Many ternary systems have been also suggested as promising electrocatalysts for oxygen evolution reaction [8,13]. However, issues as the reduction of catalyst loading and lifetime are still in a continuous research interest. Electrocatalytic films of iridium oxide deposited by magnetron sputtering technique have shown significant performance with the lowest metal loading [14,15]. In the present study iridium oxide sputtered on carbon substrate is investigated as anode catalyst in PEM water electrolyzer. The research is focused on the influence of the temperature and the access of liquid water at the electrode surface on the performance of the cell. The achieved cell performance is compared with the most efficient PEM water electrolysis systems existed [8].

2. Experimental

2.1. Working electrodes and MEA preparation

The iridium electrocatalyst under study was deposited by the dc magnetron sputtering from Ir target in Ar/O_2 plasma. The description of the main sputter device as well as the sputtering conditions which are critical for the final film formation, have been described elsewhere [16]. A hydrophobic Toray carbon paper (E-tek) covered with a 50 nm sputtered Ti layer functioned as a catalyst substrate. The addition of Ti improves the adherence of the catalytic layer to the Toray carbon paper and presumably, prevents it from oxidation at the high anodic potentials where oxygen evolution takes place thus, acting as dimensionally stable anode (DSA) [17,18]. The

* Corresponding author. Tel.: +30 2610965272; fax: +30 2610965223.
E-mail address: miranda@iceht.forth.gr (D. Labou).

0378-7753/$ – see front matter © 2008 Elsevier B.V. All rights reserved.
doi:10.1016/j.jpowsour.2008.08.013

final thickness of the sputtered film (determined on control sputtered glass substrates by profile meter) is 500 nm corresponding to Ir catalyst load 0.2 mg cm^{-2}. The membrane electrode assembly (MEA) used for the water splitting in the PEM electrolytic cell was prepared by hot pressing the hydrogen and oxygen evolution electrodes up to 120 °C at 375 kg cm^{-2} on both sides of a commercial Nafion 115 membrane (Ion Power Inc.). A thin layer of 5% Nafion solution (Aldrich) was applied prior to the pressing on the surface of the electrodes in order to improve the adherence to the Nafion membrane and the electrochemical interface. Both anode and cathode have the same geometrical area equal to 4 cm^2, while the area of the reference electrode was ~4 mm^2 and was positioned at least 5 mm away from the cathode. The corrosion resistance of the carbon substrate of the Ir electrode was compared with that of a Pt sputtered anode on carbon paper. For that reason an electrode comprising a sputtered Pt catalyst layer (500 nm) on a Toray paper carbon substrate has been prepared by magnetron sputtering as well.

2.2. Experimental techniques

The surface morphology and the particle size as well as the oxidation state of the electrocatalysts were studied by means of scanning electron microscopy (LEO SUPRA 35 VP) and X-ray photoelectron spectroscopy (XPS). The photoemission measurements were carried out in an ultra high vacuum system equipped with an easy entry specimen assembly. The photoelectrons' detector was a hemispherical analyzer (SPECS LH-10) with pass energy 97 eV. The unmonochromatized Al Kα line (1486.6 eV) was used in all XPS measurements.

The electrochemical characterization was performed in a self-built cell with two compartments, where hydrogen and oxygen evolution take place, separated by the membrane electrode assembly under study. The fabricated MEAs were sandwiched between two graphite plates with carved micro-channels for gas distribution, serving as current collectors. The cell has provisions for temperature control, humidification and flow measurements. The humidification is attained by a pair of independently heated humidifiers positioned at both sides of the cell. Helium, with a flow rate equal to 100 sccm min^{-1}, was used as a carrier gas to feed the reactant water to the anode at atmospheric pressure. The cell could be operated both under steam and liquid water conditions depending on the temperature of the anode humidifier with respect to the cell temperature. The liquid water operating mode was achieved by setting the humidifier above 90 °C while maintaining the cell's temperature at least 10 °C lower. The experiments were carried out at room and elevated (up to 90 °C) cell temperatures. The electrochemical study was performed via cyclic voltammetry and steady state polarization measurements, using a computer controlled Potentiostat/Galvanostat (EG&G Instruments Princeton Applied Research 263A) while a frequency response analyzer (EG&G 1025) was used for the IR drop determination of the

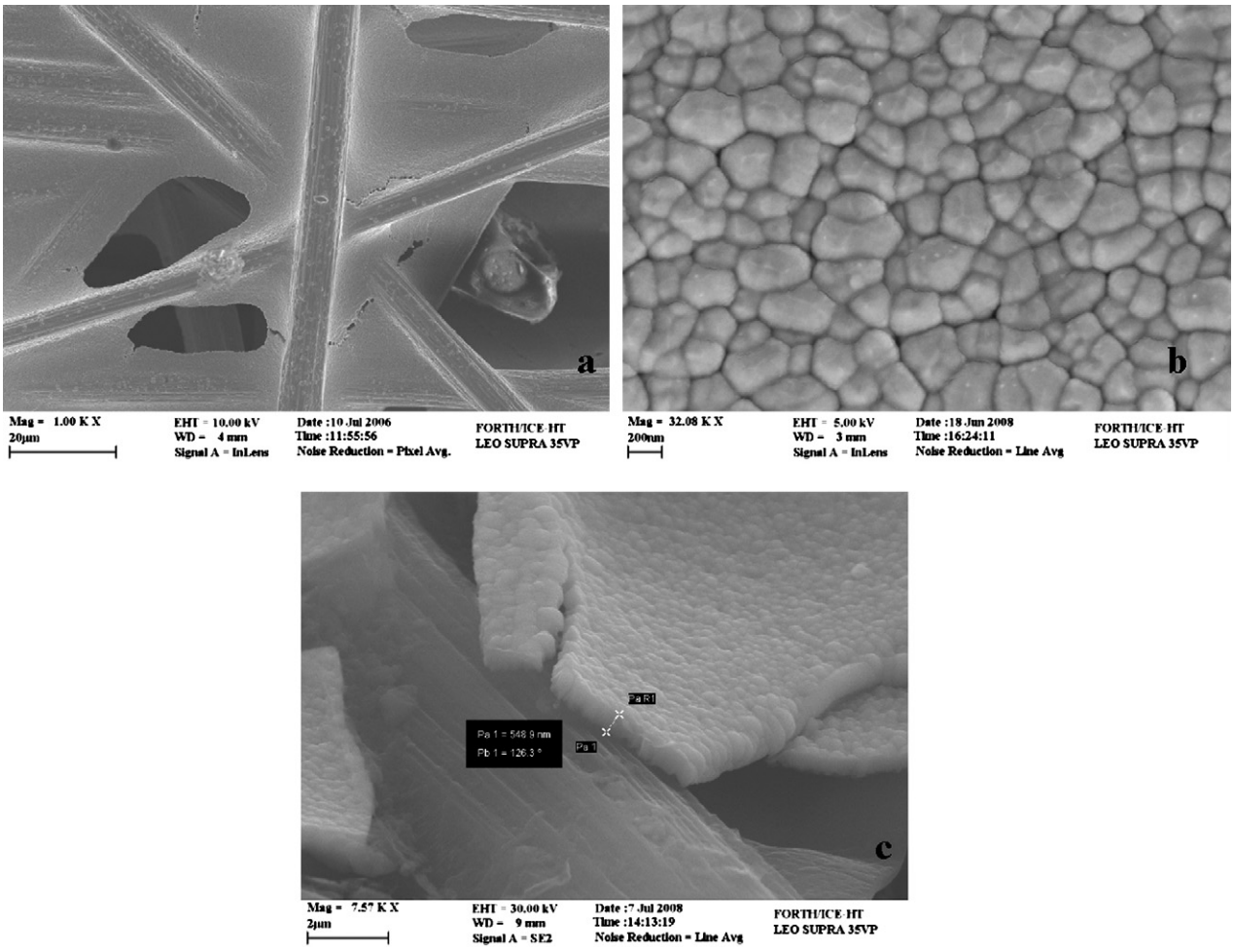

Fig. 1. The SEM images of the sputtered iridium oxide are shown the uniform coverage of the carbon fibers (a), the particle size distribution 100–300 nm (b) and the film thickness (c).

system via the ac impedance technique. The polarization curves recorded after a series of cyclic voltammograms in the potential region between hydrogen and oxygen evolution. The system was initially polarized potentiostatically up to a maximum current value and remained there for at least 5 min. Then the potential was gradually decreased backward to the open circuit value. Each point of the curve was recorded after 30 s of stabilization time. The anode's outlet was connected to a quadrapole mass spectrometer (OMNISTAR) in order to monitor the composition of the gaseous products (O_2 and CO_2) at the cell's outlet.

3. Results and discussion

The homogeneous particles distribution and the ability to deposit extremely low metal loadings constitute the main characteristics of the electrodes produced by magnetron sputtering. The SEM image of the as prepared sample (Fig. 1a) shows a well-adhered thin layer which covers the carbon fibers. The layer is nanostructure with particle size 100–300 nm (Fig. 1b) while its thickness is 500 nm (Fig. 1c).

The oxidation state of iridium on the as prepared sample was detected by the use of XPS. The spectrum of the Ir4f photoelectrons fitted by the use of XPS peak fit software (Fig. 2) testifies the presence of more than one species in the sputtered film. The fitting procedure was done by constraining the spin orbit splitting of the Ir peaks at 2.9 eV and the intensity ratio $Ir4f_{7/2}$:$Ir4f_{5/2}$ = 4/3, thus resulting in the existence of both Ir^0 and Ir^{3+} species at 60.7 and 62 eV, respectively [19,20]. Ir^0 is the most abundant species on the surface, thus showing that the preparation of the sample by magnetron sputtering results in the formation of mainly metallic Ir. The fitting procedure resulted in an additional peak at 66.7 eV, which can be associated to screening effects created after the photoemission, resulting in a positive shift of the binding energy in agreement with previous XPS studies on iridium oxides [21,22].

One of the main features of iridium metal is its ability to form multilayer (thick) oxides during continuous potentiodynamic cycling in the potential range between hydrogen adsorption and the onset of oxygen evolution ($E^{WR}_{RHE} = 1.5$ V in dilute H_2SO_4 and $HClO_4$) [23]. The formation of the iridium oxide phases is an irreversible process as they are not being reduced even by deep cathodic polarization [24,25]. This kind of activation of the sputtered iridium oxide film was attempted also in our case where the anode is interfacing a proton conductive polymer electrolyte (Nafion). Fig. 3 shows the cyclic voltammograms carried out by increasing progressively the anodic potential from 0.4 up to 1.5 V. The extension of the anodic potential limit and the continuous cycling results in the progressive oxidation of the Ir film and the diminishing of the hydrogen adsorption/desorption region giving also lower currents for the H_2 evolution. It is worth noticing that the oxidation peak of H_{ad} species at 0.1 V decreases progressively with increasing the anodic limit of the voltammograms up to 1.2 V. At higher anodic potentials the appearance of the anodic and cathodic peaks at 0.95 and 0.92 V, respectively, is accompanied by the irreversible sharp decrease of the oxidation peak of H_{ad}. Certainly this behavior can be attributed to the extensive oxidation of the Ir surface. The essentially reversible oxidation process that is being expressed through the reversible peaks at 0.95 and 0.92 V represent the chemical equilibrium between two oxidation states which coexist on the IrO_x surface. According to the literature these correspond to the equilibrium reaction that represents the reversible oxidation/reduction of Ir^{3+} to Ir^{4+} [26]. In addition, the magnitude of the oxidation and reduction peaks strongly indicates the degree of oxidation of the Ir surface. As it is shown in Fig. 4 the prolonged cycling results in the complete deactivation of the electrocatalyst with respected to H_2 activation processes, though this is only reflect to a small increase

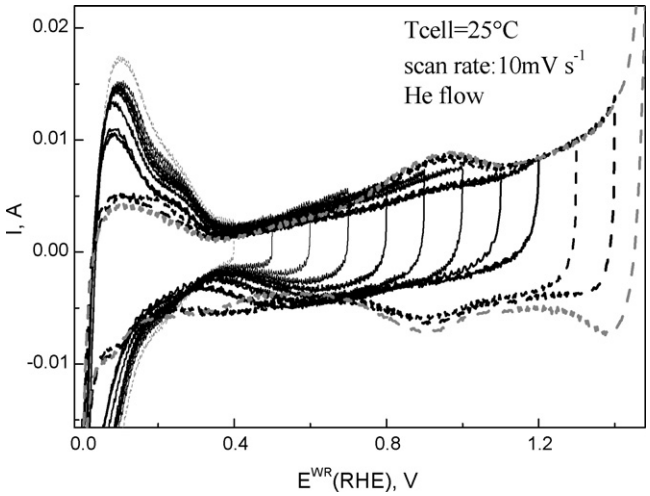

Fig. 3. Stepwise cyclic voltammograms scanned on the iridium oxide electrode at $T = 25\,^{\circ}C$. Scan rate: 10 mV s^{-1}.

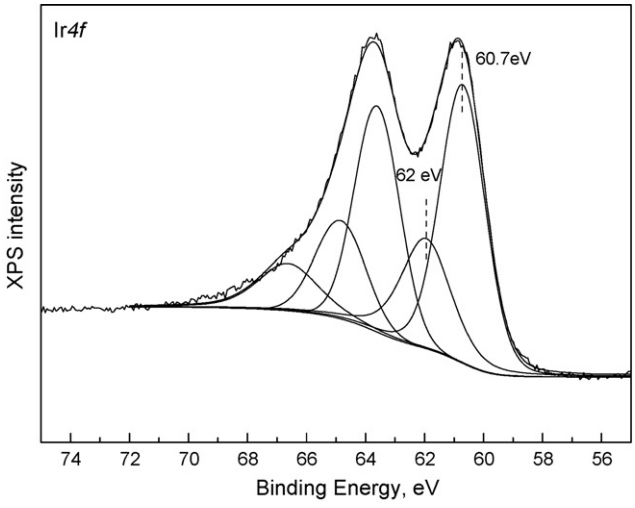

Fig. 2. The XPS Ir4f spectrum of the iridium oxide film scanned after the sputtering technique.

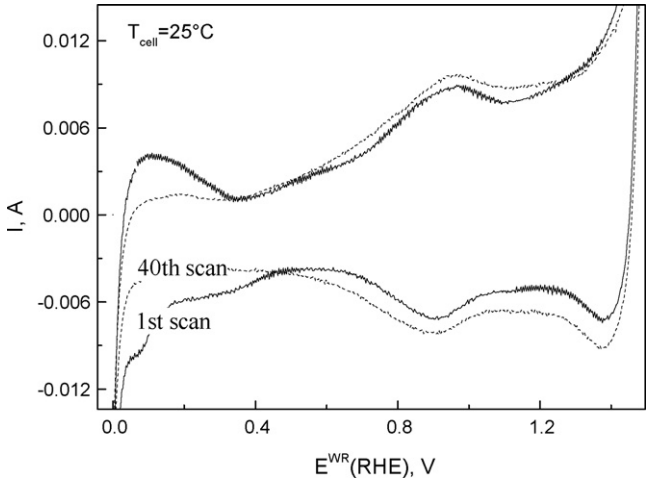

Fig. 4. Cyclic voltammograms on the iridium oxide anode carried out during the 1st and the 40th scan at $T = 25\,^{\circ}C$. Scan rate: 10 mV s^{-1}.

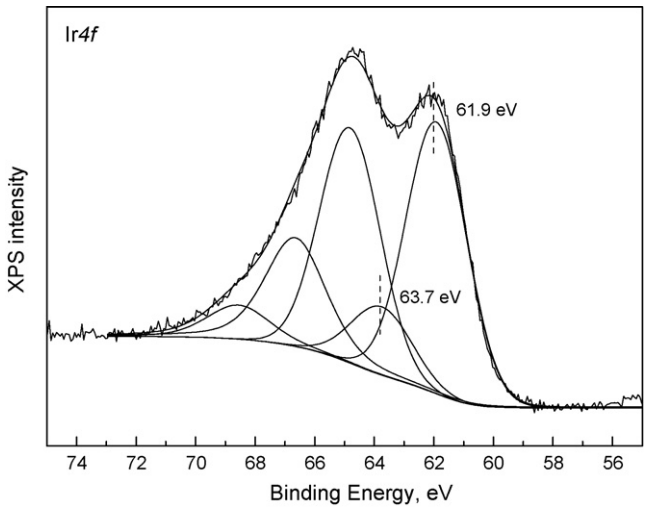

Fig. 5. The XPS Ir4f spectrum of the iridium oxide anode after the electrochemical characterization.

(~33%) of the oxidation peak at 0.95 V. The electrochemical activation of the surface is approaching steady state since the capacitive anodic charges do not change anymore through repeating cycling.

The Electrochemical Surface Area (EAS) of the as prepared Ir layer is 114 $m^2\,g^{-1}$ Ir calculated from the area of H_2 oxidation peak of the voltammogram with anodic potential limit 0.4 V (Fig. 3) according to Eq. (1) [27]:

$$\mathrm{EAS} = \frac{Q_H}{Q_{Ho} G_{Me}} \quad (1)$$

where Q_H: the charge associated with hydrogen adatoms desorption; Q_{Ho}: the charge per unit surface area corresponding to the coverage of the metal by one monolayer of hydrogen (=252 $\mu C\,cm^{-2}$ [28]); G_{Me}: the amount of Ir in the catalytic layer.

This denotes that 57% of the total Ir loading is electrochemically active, i.e. is interfacing the Nafion electrolyte. This is considered as an ideal dispersion of the electrocatalytically active surface sites approaching that of highly dispersed conventional catalytic systems. If we consider that the EAS does not change significantly during the oxidation process it is possible to compare the charge needed for the Ir^{3+} to Ir^{4+} transformation (Fig. 4) with the charge corresponds to EAS as this was estimated above. This ratio is 0.23 and it presumably indicates the equilibrium ratio of the Ir^{3+}/Ir^{4+}.

The oxidation state of the activated IrO_x was confirmed by XPS (Fig. 5) where the peaks at 61.9 and 63.7 eV, can be assigned to Ir^{3+} and Ir^{4+} or higher oxidation states, respectively, in agreement with other published data [19]. Concerning the Ir^{4+} oxidation state the $Ir4f_{5/2}$ component seems to be more intense than the $Ir4f_{7/2}$ one indicating the existence of two superimposed spectra located at the same binding energy; one attributed to $Ir4f_{5/2}$ and the other probably resulting from screening effects emanating from the spectrum of Ir^{3+} at 61.8 eV. The doublet assigned to higher than Ir^{4+} state is accompanied by a single peak at 68.08 eV which also can be assigned as a screening effect result. It is worth noticing that the ratio of the XPS peaks at 63.7 eV (Ir^{4+}) and 61.9 eV (Ir^{3+}), which was found 0.25, is almost identical to the aforementioned estimated ratio of the (Ir^{3+}/Ir^{4+}) = 0.23 derived from the cyclic voltammograms of Figs. 3 and 4. Based on these observations it can be assumed that the estimated ratio indicates the equilibrium composition of the IrO_x electrocatalytic layer.

Ti used for the better adherence of the Ir film was neither detected by the XPS before nor after electrochemical characterization probably due to its very low amount which was obscured by the thicker Ir film.

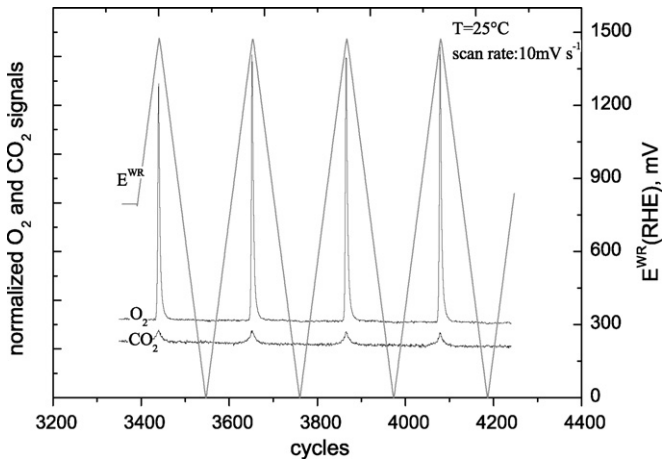

Fig. 6. Mass spectrometer signals of the iridium oxide anode outlet during cyclic voltammetry between hydrogen and oxygen evolution region at 25 °C.

The gases produced during the potentiodynamic cycles were analyzed via a mass spectrometer connected to the outlet of the anode compartment. The corresponding mass signals at the anode with respect to the applied potential are shown in Fig. 6. The onset potential of the oxygen evolution reaction at 1.3 V (25 °C) has been accompanied by CO_2 production, which is the main by-product of this reaction on carbon-based electrodes. However, the CO_2 produced from the iridium oxide electrode is much less in quantity in comparison to the massive CO_2 production during the O_2 evolution on Pt sputtered film (Fig. 7). As it is evidently depicted in MS signal shown in Fig. 7 almost no oxygen is detected while it massively reacts with the carbon substrate to form CO_2. The minimal corrosion behavior observed in the case of the Ir electrode can be plausibly attributed either to the Ti thin layer (50-nm thick) that was initially deposited on the carbon Toray paper or to the catalytic activity of the O species that are being formed on the IrO_x surface. Certainly the massive formation of CO_2 in the case of Pt electrode strongly indicates that the adsorbed oxidic species on the Pt surface are very active towards the catalytic or electrocatalytic oxidation of the carbon support at the boundaries of the Pt/C particles. Although Pt catalysts are not considered as an efficient anode in OER however, it can play an essential role in the promising field of regenerative fuel cells as a component in binary and ternary bifunctional electro-

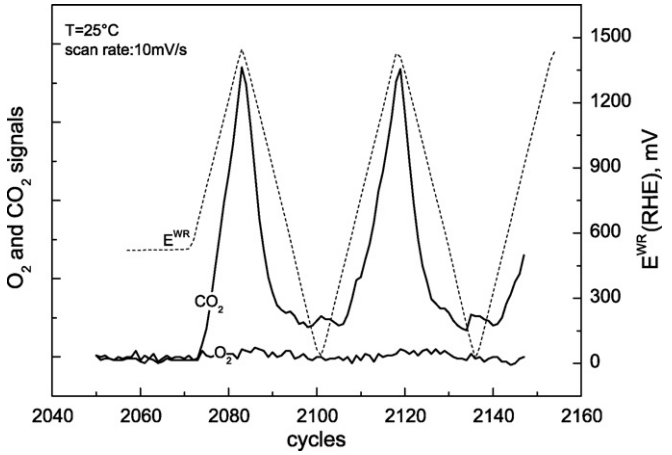

Fig. 7. Mass spectrometer signals of the Pt oxide anode outlet during cyclic voltammetry between hydrogen and oxygen evolution region.

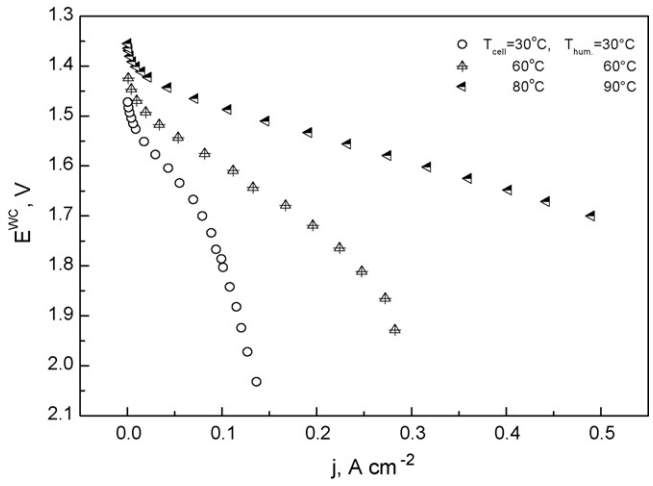

Fig. 8. Polarization curves of the PEM electrolyzer at different cell temperatures (T_{cell}) under water *steam* feed.

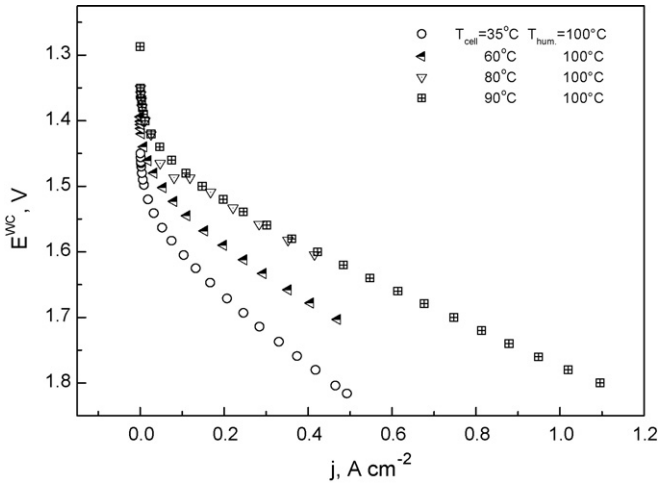

Fig. 9. Polarization curves of the PEM electrolyzer at different cell temperatures (T_{cell}) under *condensate* water feed.

catalytic systems [29,30]. It must be stressed that the comparative experiments depicted in Figs. 6 and 7 cannot replace any long-term testing which is the necessary proof for the electrode's long-term stability.

The performance of the iridium oxide as an anode for OER was examined in the PEM test cell by recording steady state polarization curves at different operating temperatures. The polarization curves were recorded after a series of cyclic voltammograms in the potential region between hydrogen and oxygen evolution. The system was initially polarized potentiostatically up to a maximum current value and remained there for at least 5 min. Then the potential was gradually decreased backwards toward the open circuit value. Each point of the curve was recorded after 60 s of stabilization time.

The effect of the anode temperature on the cell performance when the humidifier's temperature follows the cell working temperature is shown in Fig. 8. Generally, the increase of the cell temperature improves performance. At lower temperatures limiting current is observed at higher cell potentials although the steam flow was by a factor of three higher than the observed limiting currents. This behavior certainly denotes a strong kinetic effect of the partial pressure of water on the anodic electrocatalytic water splitting. With the cell's and humidifier's temperatures being at 80 and 90 °C, respectively, a current density of 0.5 A cm^{-2} was measured at 1.7 V. However, if the humidifier's temperature is controlled at 100 °C so the operating temperature of the cell is lower, the steam condensates inside the cell, thus resulting in a dramatic enhancement of the cell's performance. This effect is depicted by the polarization curves in Fig. 9. By comparing the polarization curves in Figs. 8 and 9 at cell's temperature of 80 °C it is evident that the current density is almost double when the humidifier's temperature is set at 100 °C. Definitely, the observed efficiency improvement is due to the presence of liquid water on the anode surface. Beyond the kinetic effect of the higher water activity, being in the liquid form, the condensate water molecules must enhance the accessibility of the electrolyte to isolated parts of iridium oxide surface, thus increasing the electrochemical interface. Based on this option, a maximum current density of 1.1 A cm^{-2} at 1.8 V and 90 °C has been achieved (Fig. 9), which is among the best efficiencies reported on iridium anodes with the lowest metal loading according to the recent PEM electrolyzer literature. The highest performance is given by Marshall et al. [8] where the measured current density per mg of catalyst was 0.5 A mg^{-1} at 1.56 V and 80 °C by using an $Ir_{0.6}Ru_{0.4}O_2$|Nafion 115|Pt/C electrolyzer. The aforementioned value corresponds to the reported surface area current density of 1 A cm^{-2} and was calculated taking into consideration that the reported metal loading in Ref. [8] is 2 mg cm^{-2}. Nevertheless they reported instabilities in the cell performance due to passivation of the Ti backings. In order to compare the present performance with the results of Ref. [8] the IR free cell potential was estimated. Marshall et al., mentioned an IR drop value of 150 mV at 1 A cm^{-2}. Taking into consideration the high current part (ohmic) of their *I–V* curves in (Fig. 4 of the Ref. [8]) the IR drop must not be higher than 130 mV at 1 A cm^{-2}. Thus, the IR drop free cell potential at the aforementioned current density is at least 1.43 and 1.5 V for the cases of $Ir_{0.6}Ru_{0.4}O_2$ and IrO_2, respectively. In the present study the IR free cell potential that corresponds to a surface area current density of 1 A cm^{-2} is estimated around 1.51 V. The IR correction was based on ac impedance measurements of the cell, where the total ohmic resistance including the ionic resistance of the electrolyte and the electronic and conduct resistances of the bipolar plates and leading wires was determined 66 mΩ. It is obvious that the present results compare quite well with those of IrO_2 electrodes reported by Marshall et al. [8] although in the present study the amount of catalyst used is 10 times less in comparison to the amount used in Ref. [8]. The yielded performance, at 1.1 A cm^{-2} and E_{cell} = 1.8 V, translated into energy consumption is equal to 4.24 kWh Nm^{-3} H_2. Taking into consideration that the thermoneutral voltage at 90 °C is E_{th} = 1.48 V, then according to the aforementioned energy consumption the thermal energy efficiency is 83%. However, this suffers from the IR drop due to the high contact resistances resulted by the hand made electrolytic cell. By subtracting the IR losses from the cell's voltage value the energy consumption decreases to 3.62 kWh Nm^{-3} H_2 with cell efficiency 98%.

4. Conclusions

The commercial development of PEM electrolyzers can be expanded through material cost optimization and design simplicity. An important step towards the reduction of electrocatalyst's load is the concept of using the magnetron sputtering technique. In the present work we have demonstrated the efficient use of iridium oxide sputtered films on carbon substrates as electrodes for the OER. The cell efficiency attained at 1 A cm^{-2} is 83% while the ohmic free efficiency has been estimated 98% (ohmic free E_{cell} = 1.51 V) for catalyst loading 0.2 mg cm^{-2}. The observed efficiency is in congruence with the published best efficiency on pure IrO_2 anode although in the present study the catalyst loading is 10 times lower. The com-

parative study of Pt and Ir electrodes has shown that the superiority of IrO_x can be attributed to the different nature and activity of the oxidic species as the precursor for O_2 evolution reaction. The main feature of these oxidic species is their low oxidative reactivity with the carbon substrate as compared to Pt electrode.

Since generally OER proceeds more efficiently on mixed Ir–Ru oxides, further work should be directed in the measurement of the performance of low loading bimetallic systems prepared by magnetron sputtering technique and on prolonged stability tests.

Acknowledgement

This paper has been supported by and carried out within EU project 'Prometheas', Contract Nr ICA2-2001-10037 and by GSRT, Ministry for Development of Greece in the framework of the bilateral project GR-BG, Contract Nr 098G.

References

[1] R. Wurster, J. Schindler, in: W. Vielstich, A. Lamm, H.A. Gasteiger (Eds.), Handbook of Fuel Cells, Fundamentals Technology and Applications, vol. 3, John Wiley & Sons Ltd., West Sussex, England, 2003.
[2] S.A. Grigoriev, V.I. Porembsky, V.N. Fateev, Int. J. Hydrogen Energy 31 (2006) 171.
[3] E. Rasten, G. Hagen, R. Tunold, Electrochim. Acta 48 (2003) 3945.
[4] A. Marshall, B. Børresen, G. Hagen, M. Tsypkin, R. Tunold, Electrochim. Acta 51 (2006) 3161.
[5] F. Andolfatto, R. Durand, A. Michas, P. Millet, P. Stevens, Int. J. Hydrogen Energy 19 (1994) 421.
[6] M. Kondoh, N. Yokoyama, C. Inazumi, S. Maezawa, N. Fujiwara, Y. Nishimara, K. Oguro, H. Takenaka, J. New Mater. Electrochem. Syst. 3 (2000) 61.
[7] K. Ledjeff, F. Mahlendorf, V. Peinecke, A. Heinzel, Electrochim. Acta 40 (1995) 315.
[8] A.T. Marshall, S. Sunde, M. Tsypkin, R. Tunold, Int. J. Hydrogen Energy 32 (2007) 2320.
[9] E. Rasten, PhD Thesis, Electrocatalysis in water electrolysis with solid polymer electrolyte NTNU, Trondheim, Norway, 2001.
[10] T. Ioroi, N. Kitazawa, K. Yasuda, Y. Yamamoto, H. Takenaka, J. Electrochem. Soc. 147 (2000) 6.
[11] V. Baglio, A. Di Blasi, T. Denaro, V. Antonucci, A.S. Aricó, R. Ornelas, F. Matteucci, G. Alonso, L. Morales, G. Orozzo, L.G. Arriaga, J. New Mater. Electrochem. Syst. 11 (2008) 105.
[12] F.I. Mattos-Costa, P. de Lima-Neto, S.A.S. Machado, L.A. Avaca, Electrochim. Acta 44 (1998) 1515.
[13] X. Chen, G. Chen, Electrochim. Acta 50 (2005) 4155.
[14] G. Beni, L.M. Schiavone, J.L. Shay, W.C. Dautremont-Smith, B.S. Schneider, Nature 282 (1979) 281.
[15] E. Slavcheva, I. Radev, G. Topalov, E. Budevski, Electrochim. Acta 52 (2007) 3889.
[16] E. Slavcheva, U. Schnakenberg, W. Mokwa, Appl. Surf. Sci. 253 (2006) 1964.
[17] H. Beer, Improvements in or relating to electrodes for electrolysis, British Patent 1,147,442, 1969.
[18] S. Trasatti, Electrochim. Acta 45 (2000) 2377.
[19] L.A. da Silva, V.A. Alves, S.C. de Castro, J.F.C. Boodts, Colloid Surf. A: Physicochem. Eng. Aspects 170 (2000) 119.
[20] V. Boissel, S. Tahir, C.A. Koh, Appl. Catal. B: Environ. 64 (2006) 234.
[21] L. Atanasoska, R. Atanasoski, S. Trasatti, Vacuum 40 (1990) 91.
[22] Q. Fu, T. Wagner, Surf. Sci. Rep. 62 (2007) 431.
[23] L.D. Burke, D.P. Whelan, J. Electroanal. Chem. 162 (1984) 121.
[24] D.A.J. Rand, R. Woods, J. Electroanal. Chem. 55 (1974) 375.
[25] S. Gottesfeld, S. Srinivasan, J. Electroanal. Chem. 86 (1978) 89.
[26] C. Bock, V.I. Birss, J. Electroanal. Chem. 475 (1999) 20.
[27] S.A. Grigoriev, P. Millet, V.N. Fateev, J. Power Sources 177 (2008) 281.
[28] L.-J. Wan, M. Hara, J. Inukai, K. Itaya, J. Phys. Chem. B 103 (1999) 6978.
[29] W. Yao, J. Yang, J. Wang, Y. Nuli, Electrochem. Commun. 9 (2007) 1024.
[30] J. Pettersson, B. Ramsey, D. Harrison, J. Power Sources 157 (2006) 28.